Dalton Transactions

ROYAL SOCIETY OF CHEMISTRY

PAPER

View Article Online
View Journal | View Issue

Cite this: *Dalton Trans.*, 2023, **52**, 4044

Fluorine-based Zn salan complexes†

Nsikak B. Essien, [a] Antal Galvácsi,[b] Csilla Kállay, [b] Youssra Al-Hilaly, [c,g] Ramón González-Méndez, [a] Geoffrey R. Akien, [d] Graham J. Tizzard,[e] Simon J. Coles, [e] Maria Besora [*f] and George E. Kostakis [*a]

Received 21st December 2022,
Accepted 20th February 2023

DOI: 10.1039/d2dt04082d

rsc.li/dalton

We synthesised and characterised the racemic and chiral versions of two Zn salan fluorine-based complexes from commercially available materials. The complexes are susceptible to absorbing H_2O from the atmosphere. In solution (DMSO–H_2O) and at the millimolar level, experimental and theoretical studies identify that these complexes exist in a dimeric-monomeric equilibrium. We also investigated their ability to sense amines *via* ^{19}F NMR. In $CDCl_3$ or d^6-DMSO, strongly coordinating molecules (H_2O or DMSO) are the limiting factor in using these easy-to-make complexes as chemosensory platforms since their exchange with analytes requires an extreme excess of the latter.

Introduction

A compound is considered chiral when it exists in two or more asymmetric forms with non-superimposable mirror images without changing its bond orders, atom–atom connections, and atomic compositions and these forms are called enantiomers.[1] Nature is full of chiral components such as amino acids, saccharides, peptides, enzymes, and proteins,[2] while many chiral compounds in the pharmaceutical industry and material sciences possess biological activity.[3,4] The enantiomeric synthesis of asymmetric compounds has rapidly increased over the years,[5] and more complicated and sophisticated systems have been developed.[6] For example, enzymes are used as catalysts to promote organic transformations,[7] chiral compounds are used in different stages of drug discovery[8,9] and amino acids are used as building blocks for larger molecules *i.e.* protein, nucleic acid, and components of food and beverages.[10]

Enantiomers have the same physical properties in an achiral environment, but may possess different pharmacological and biological activities.[11] Conventional high-performance liquid chromatography (HPLC) can separate the enantiomers,[12] but this approach involves costly chiral columns. Thus, developing new methods for enantiomeric discrimination is highly interesting for industrial and biomedical applications and is subsequently vital for future discoveries.[13] For example, circular dichroism (CD) and fluorescence,[14–21] monitor absorbance intensity change(s) whereas Nuclear Magnetic Resonance (NMR) proceeds chemically shifted signals;[22–25] these methods rely on host-guest interaction(s); therefore, thermodynamic and kinetic parameters and equipment's response time signify method applicability and limitation. In the latter case, methods incorporating chiral templates and ^{1}H-NMR are popular,[26–31] however, lately, emphasis is given to developing hetero nuclear-based methods *i.e.* ^{31}P[24,32] or ^{19}F.[33–35] The latter method has the following two advantages: lack of background interference;[33,34] thus applies to large molecules, such as proteins,[35,36] and a broad detection window from −200 ppm to 200 ppm depending on the transducers, *i.e.* $-CF_3$, $-OCF_3$, –F and other groups.[37] Pioneer works from Swager[38,39] and Song[40] establish the principles in using new or modifying already known chiral fluorine-based complexes for discriminating chiral amine-based methods. Both methods use non-labile, less abundant, toxic elements, work in non-coordinating solvents and rely on the host-guest interaction principle; thus, two different peaks (one for the complex and one for the complex + analyte in 1 : 1 ratio) appear in the ^{19}F NMR spectrum. In the latter case,[40] the method also applies to coordinating solvents, and its operational window is 0.21 ppm.

The condensation reaction of salicylic aldehyde and ethylenediamine yields the well-known versatile salen framework

[a]*Department of Chemistry, School of Life Sciences, University of Sussex, Brighton BN1 9QJ, UK. E-mail: G.Kostakis@sussex.ac.uk*
[b]*Department of Inorganic and Analytical Chemistry, University of Debrecen, H-4032 Debrecen, Hungary*
[c]*Sussex Neuroscience, School of Life Sciences, University of Sussex, Brighton BN1 9QG, UK*
[d]*Department of Chemistry, Lancaster University, Lancaster LA1 4YB, UK*
[e]*UK National Crystallography Service, Chemistry, University of Southampton, Southampton SO1 71BJ, UK*
[f]*Departament de Química Física i Inorgànica, Universitat Rovira i Virgili, C/Marcel lí Domingo, 1, 43007 Tarragona, Spain. E-mail: maria.besora@urv.cat*
[g]*Chemistry Department, College of Science, Mustansiriyah University, Baghdad, Iraq*

†Electronic supplementary information (ESI) available. CCDC 2231658–2231663. For ESI and crystallographic data in CIF or other electronic format see DOI: https://doi.org/10.1039/d2dt04082d

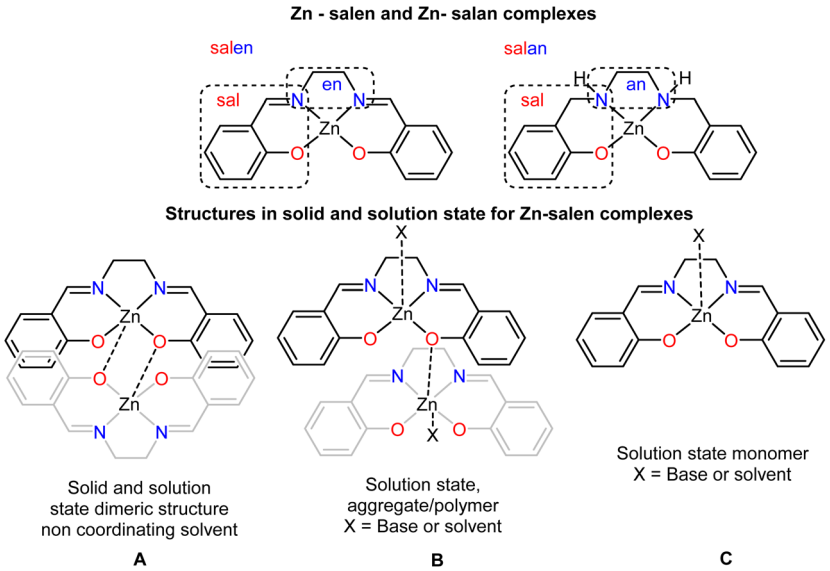

Scheme 1 (Upper) the differentiation of salen and salan framework (middle) possible structures in solid and solution (lower) possible species for sensing processes.

(Scheme 1, upper), which has been extensively used to produce complexes with applications in catalysis and sensing.[41–55] From the synthetic perspective, the corresponding Zn complexes crystallise as dimers (Scheme 1, **A**); however, in solution, they either form monomers (Scheme 1, **C**) in coordinating solvents or the presence of a base or aggregates (Scheme 1, **B**), non-coordinating solvents. The former process is well and explicitly discussed and recently reviewed by Di Bella.[52,56] In these reviews, the coordination number that the metal centre adopts depends on the solvent system and the presence (absence) of substrates, varying from four to six. Notably, the reduced version of salen, which means salan ligands (Scheme 1, upper right) and their corresponding Zn complexes, have been less investigated.[57–64] These compounds are susceptible to oxidative dehydrogenation, depending on the solvent medium.[65,66] Only 31 crystal structures have been deposited in the CSD.[67] The sp^3 carbon atoms of the salan framework impose flexibility and, consequently, possible alterations in the geometry of the metal centre, deviating from the dominant square planar and/or square pyramidal conformation.

Previous studies identify the ability of Zn(II) complexes to sense biologically important small molecules[68] such as amino acids,[69,70] amines,[71] saccharides[72,73] and ribonucleosides.[74] Recently, Zhao suggested that Zn(II) salen complexes, ideal models for catalysis, are inappropriate for sensing purposes because their structural changes (Scheme 2, species **A′**, **B′** and **C′**) interfere chronically with the sensing process, thereby averaging the ^{19}F NMR signals of the interconverting species.[75] With all these in mind, we embarked on a project examining if the easy-to-make, low-cost, chiral Zn(II) salan complexes can be used as chemosensory platforms with ^{19}F NMR. We detail our ligand-complex design criteria for this purpose (Scheme 2). The use of salan frameworks will increase the flexibility of the organic framework and consequently affect the coordination geometry of the metal centre. However, incorporating the rigid cyclohexane backbone instead of the en moiety will impede the flexible character. Next, we wanted to investigate the impact of the different transducers (F *vs.* OCF_3) but also varying its position, adjacent or away from the sensing point (metal centre). Thirdly, we investigated if altering the chirality of the host will impact the sensing process. Lastly, we envisaged these complexes existing as dimers in the solid state and possibly in the solution state; therefore, we hypothesised that saturated analyte (complex: analyte ratios 1 : 20, 1 : 40, 1 : 50 and above) solutions will favour the sole formation of species **C′** (Scheme 2), thus advancing a new sensing process (appearance of one peak corresponding to the complex + analyte species **C′**); the scope of this hypothesis is discussed and presented.

Results

Synthesis of the ligands

All ligands can be synthesised using commercially available chemicals in two high-yielding steps, avoiding column chromatography (Scheme 3). The ligands have been characterised by NMR (^{1}H, ^{13}C, ^{19}F), IR, UV-Vis, and HR-MS (with ESI† as an ion source). The chirality of each species has been determined by Circular Dichroism (CD) (Fig. 1), observing the opposite enantiomer. The total yield for the ligands varies between 78–98%.

Complex synthesis

With the ligands in hand and bulk, we performed several reactions for synthesising the corresponding Zn complexes

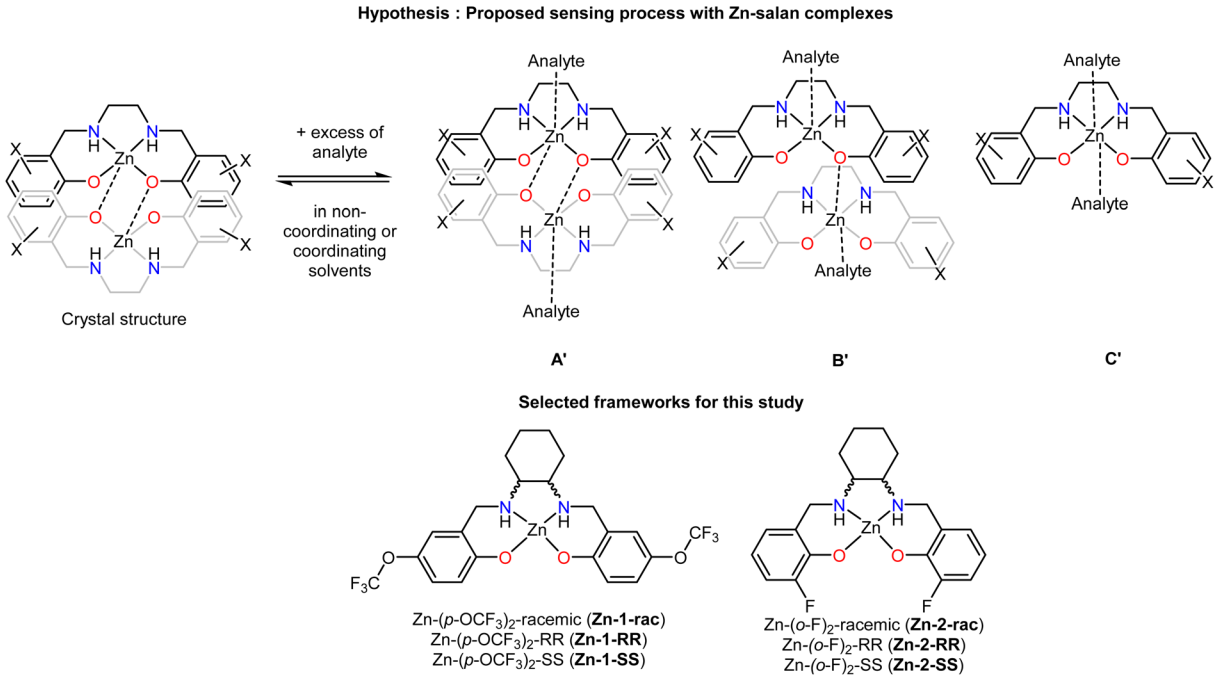

Scheme 2 (Upper) a schematic representation of the hypothesis (lower) the selected two frameworks for this study.

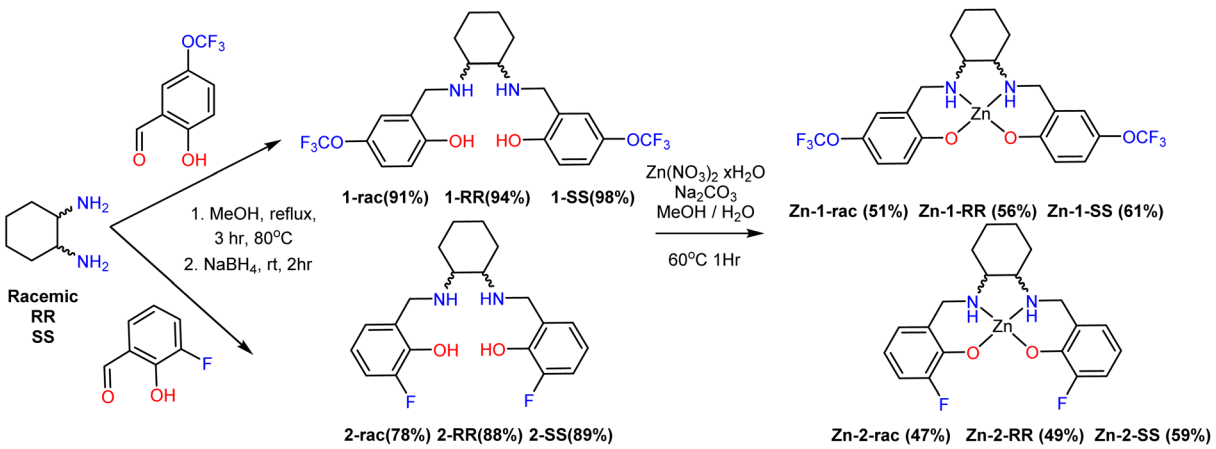

Scheme 3 A simplified version of the synthetic routes to yield all ligands and complexes.

(Scheme 3). We screened several parameters such as metal salt $Zn(NO_3)_2$ $6(H_2O)$, $ZnCl_2$, $Zn(OTf)_2$, $Zn(BF_4)_2$, $Zn(ClO_4)_2$, solvent (MeOH, CH_2Cl_2, EtOH, CH_3CN), metal : ligand ratio (3 : 1 to 1 : 3), temperature (25 °C, 50 °C, 75 °C), base (Et_3N, Na_2CO_3, K_2CO_3) and identified the optimum conditions as: $Zn(NO_3)_2$ $6(H_2O)$: Ligand : Na_2CO_3 in a molar ratio 1 : 1 : 1, on a mixture of solvents MeOH/H_2O (10/2 mL). The metal salt and ligand were dissolved in methanol, and the solution turned milky upon adding an aqueous Na_2CO_3 solution. After 1 h of reflux, the solution was filtered, and the filtrate was kept for slow evaporation. Shiny block-shaped colourless crystals were collected in good to moderate yields between four and fourteen days.

Characterisation in solid state

Single crystal X-Ray diffraction studies (Table S1†) for **Zn-1** and **Zn-2** families identified the formation of dimers for all cases (Fig. 2); however, minor differentiations could be identified in the crystallised lattice molecules for **Zn-1-*RR*** and **Zn-1-*SS***. No lattice molecules could be determined for compound **Zn-1-*rac***, however the actual formula for **Zn-1-*RR*** is [ZnL 1(CH_3OH) 0.375(H_2O)] and for **Zn-1-*SS*** is [ZnL 2(CH_3OH)]. For the **Zn-2** family, all compounds crystallise as [ZnL 2(H_2O)]. All lattice molecules form hydrogen bonding interactions with the metalloligand (ZnL) moieties. **Zn-1-*rac*** and **Zn-2-*rac*** crystallise in achiral space groups ($P2_1/n$ and $P\bar{1}$), while the remaining four

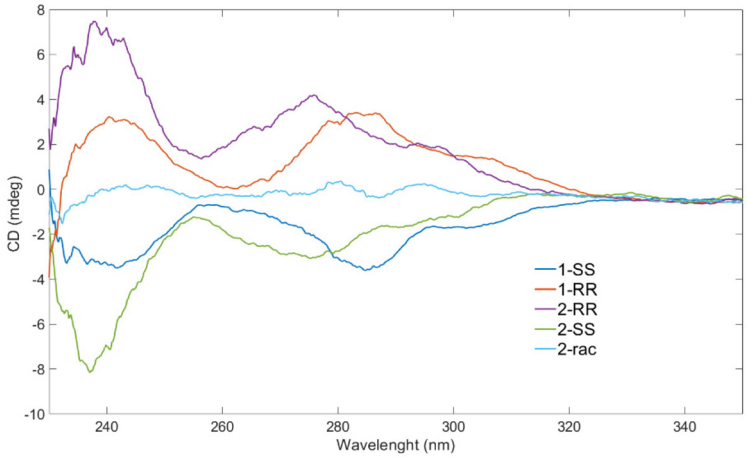

Fig. 1 The circular dichroism spectra for the ligands (solvent, MeOH, c = 1 mM, T = 298 K).

Table 1 Selected bond distances for all complexes and trigonality index

	Zn–O1	Zn–O2	Zn–O3	Zn–N1	Zn–N2	Trigonality index (τ)[77]
Zn-1-*rac*	2.057(3)	2.068(3)	1.963(3)	2.110(4)	2.141(3)	0.68
Zn-1-*RR*	2.079(7)	1.987(7)	1.990(8)	2.132(8)	2.186(8)	0.61
	1.985(8)	2.108(7)	1.987(7)	2.101(8)	2.189(8)	0.65
Zn-1-*SS*	2.088(5)	2.002(5)	1.981(6)	2.132(7)	2.190(6)	0.61
	1.995(5)	2.086(5)	1.966(6)	2.194(7)	2.126(8)	0.60
Zn-2-*rac*	1.959(4)	2.049(4)	2.101(4)	2.141(5)	2.093(5)	0.61
Zn-2-*RR*	1.959(4)	2.095(5)	2.040(4)	2.149(5)	2.109(5)	0.74
	2.051(4)	2.099(5)	1.950(4)	2.115(5)	2.133(5)	0.50
Zn-2-*SS*	1.954(5)	2.099(6)	2.051(5)	2.133(7)	2.111(6)	0.50
	2.046(5)	2.097(6)	1.959(5)	2.111(6)	2.152(7)	0.74

Trigonality index indicates the geometry of the coordination center.[77] When τ = 0 the geometry corresponds to square pyramidal, when τ = 1 corresponds to trigonal bipyramidal.

complexes crystallise in chiral space groups. The Zn centre inclines to adopt a trigonal bipyramidal geometry (Fig. S1† & Table 1). Notably, for the chiral species, two different indexes could be determined; however, their average is close to the index calculated for the non-chiral species (Table 1). In all species, the C–N bond is within the range of single bond values, discarding the occurrence of oxidative dehydrogenation,[65,76] while the phenoxido C–O bond is within the range of a single bond value. The Flack parameter value (Table S1†) for all four compounds is close to zero, thus determining enantiomeric purity. The compounds were further characterised by Thermogravimetric (TG) and elemental (CHN) analysis, which slightly deviated from the expected calculated values. They are consistent with additional lattice solvent molecules (Fig S2†).

Characterisation in solution state

With the complexes in hand, we attempted to elucidate if they retain their structure in solution; therefore, we recorded ^{1}H and ^{19}F NMR, CD and ESI-MS. The ESI-MS data for **Zn-1-*RR*** (Fig. S3†) validate the formation of monomeric and dimeric species; a characteristic peak with corresponding isotropic distribution can be identified for both species. CD studies of selected samples in DMSO validate the retention of the enantiomeric form (Fig. 3A). Then, we recorded ^{1}H and ^{19}F NMR data using a coordinating solvent (d^{6}-DMSO) and compared them with the free ligands (Fig. 3B, C and ESI†). From these data, complexation is evident; characteristic peaks in the aromatic and cyclohexane backbone regions shift at different values in ^{1}H NMR. In ^{19}F NMR, the sole peak shifts by 0.1 ppm (Fig. 3C), whereas for the **Zn-2** family, the peak shifts almost by 1 ppm (0.87 ppm, Fig. S5†). Minor peaks can be observed in the ^{1}H NMR of **Zn-1-*SS***; however, this may be attributed to different species formed in solution (see Scheme 2, **A′**, **B′** and **C′**), rather than impurities since the ^{19}F NMR data suggests the presence of only one species. To validate the existence of a monomeric or a dimeric species, we performed ^{19}F NMR diffusion studies (Fig. 3D). However, the data was inconclusive as the apparent molecular weight was intermediate between the putative monomeric and dimeric species.[78]

We performed potentiometric studies for **2-*rac*** and its corresponding **Zn-2-*rac*** complex at a millimolar level in two

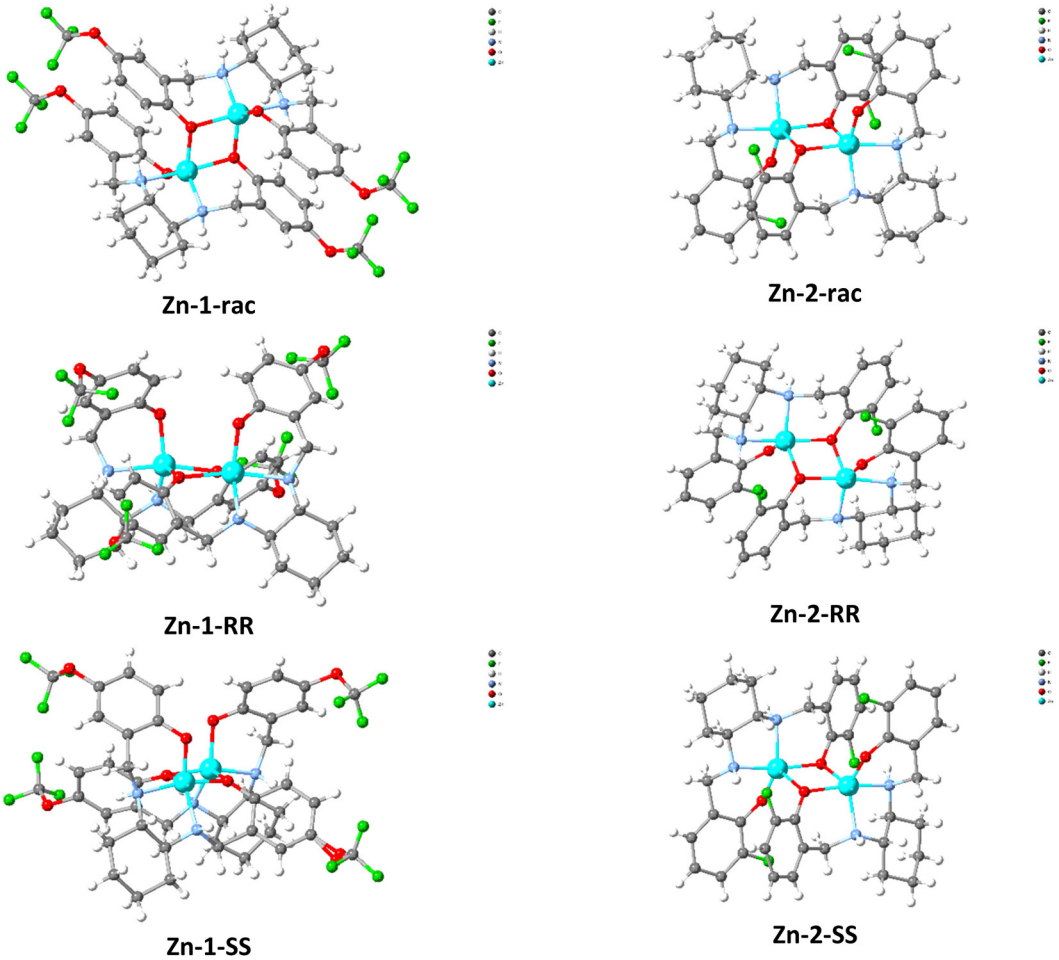

Fig. 2 Crystallographic representation of **Zn-1** (left)and **Zn-2** (right) families. Lattice solvent molecules have been omitted for clarity. Colour code; Zn (light blue), O (red), N (blue), C (grey), H (white), F (green).

concentrations (0.2 and 1.2 mM) in a mixed DMSO–H_2O solvent system (Fig. S6†). Four deprotonation constants can be calculated for the two phenolic OH and two NH groups. The lowest p*K* value belongs to the deprotonation of one NH group, while the other deprotonation processes overlap. The lowest p*K* values in all measurements agree; however, the basic pH range values slightly differ in the samples with different ligand concentrations. The solution at 1.2 mM concentration becomes turbid above pH 9, prohibiting further evaluation. The higher p*K* values were set from the 0.2 mM measurements. The interaction of the ligand with Zn(II) was studied at a 1 : 2 metal-to-ligand ratio in 0.2 and 1.2 mM (for the ligand) solutions; the data were evaluated considering the monomeric and dimeric species (Fig. 4). From the distribution curves (Table 2), we note that (a) the higher ligand concentration shifts the complex formation to lower pH, and (b) the formation of the diprotonated dimeric complex in the 1.2 mM solution is favoured. Notably, upon ligand concentration increase, the data fitting improves with the dimeric model, and at a concentration of 1.2 mM, the formation of the dimeric complex is more favourable.

Investigating amine response

With the complexes in hand, we attempted to identify the best solvent system, with $CDCl_3$ being our first choice. Previous works used this solvent and the complexes at 1 mM level.[38–40] The data presented herein are the outcome of mixing the analyte and the complex within the NMR tube, avoiding stirring or sonication for prolonged periods; the reason for this choice is our aim to develop an efficient, convenient and rapid sensing method. Our first trial for **Zn-1-*RR*** (Fig. S7†), identifies that this non-coordinating solvent system levies monomeric-dimeric competition,[52] therefore, we discarded its use. Then we used a binary solvent system ($CDCl_3$–DMSO) in different ratios. However, the same behaviour was observed again (results are not presented). Thus, we concluded that DMSO would be the ideal solvent to proceed. The ^{19}F NMR data of the complexes (Fig. 4) identify a single broad peak, indicating that an equilibrium (monomer *vs.* dimer) is favoured or that different types of interactions occur.[36] Initial studies of the complex : analyte in 1 : 1 to 1 : 4 ratios give an unaltered complex spectrum (results not presented). To our disappoint-

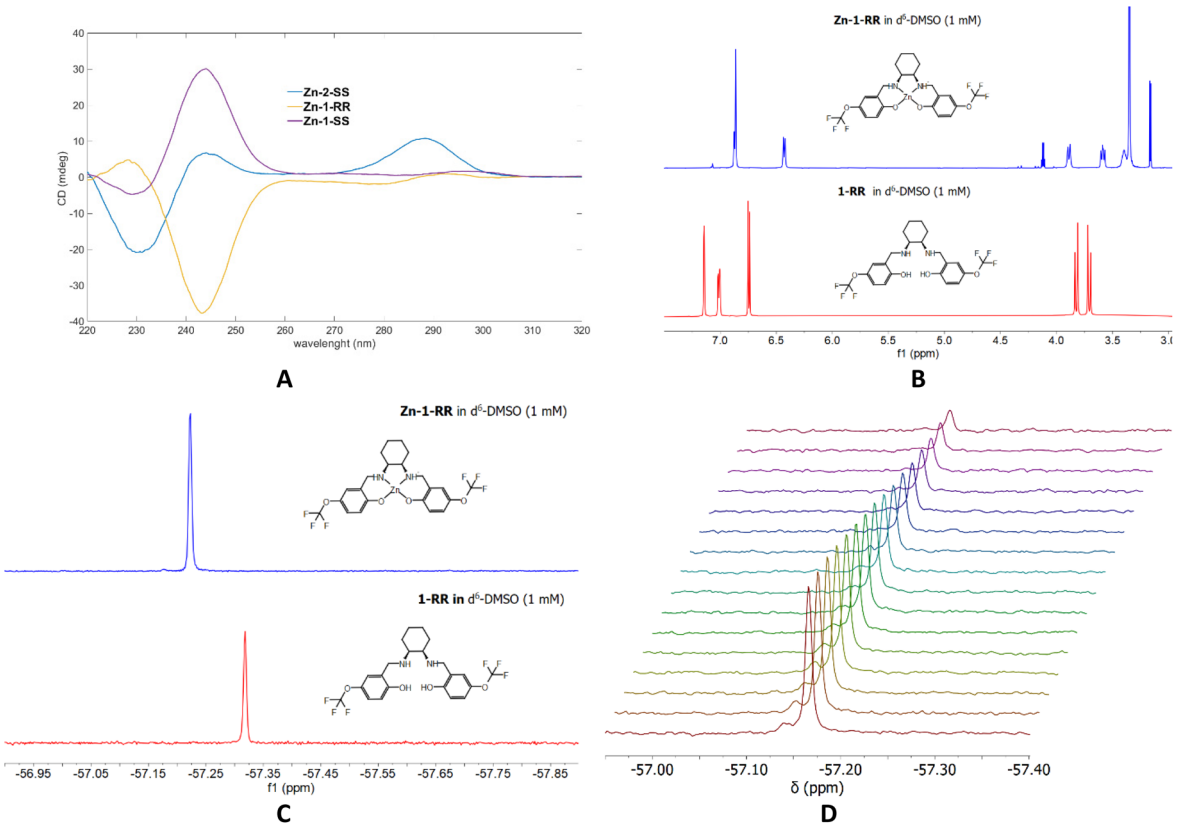

Fig. 3 (A) the circular dichroism spectra for selected complexes **Zn-1-*RR***, **Zn-1-*SS*** and **Zn-2-*SS***. (c = 1 mM) (B & C) ^{1}H and ^{19}F NMR comparison of **1-*RR*** and **Zn-1-*RR*** in d^{6}-DMSO (c = 1 mM, T = 303 K). (D) ^{19}F NMR diffusion studies.

ment, titrations of **Zn-1-*RR*** and **Zn-1-*SS*** at millimolar scale with limited excess of phenylglycinol in ratios 1 : 5 to 1 : 50, as this was our testing hypothesis, show minimal differences, thus prohibiting us from further continuing with this study. Given that we incorporated a strongly coordinating solvent (DMSO) which may occupy the coordinating site(s) on the Zn centre, we tried experiments with 1 : 100 and 1 : 150 ratios to favour the DMSO-analyte exchange. The latter experiment (1 : 150) suggests that a ligand (**1-*RR*** *vs.* analyte) exchange process starts, and the Zn(analyte)$_x$ complex forms (Scheme 1).

Then we tested **Zn-1*SS*** with other amines (Fig. 5A–C). Our first choice was to incorporate a diamine at different ratios (1 : 20, 1 : 50 and 1 : 100, Fig. 5A). The data from the first trial shows the main peak slightly shifted and two minor peaks, which could be indicative of the formation of the complex + analyte species; however, given that none of the two peaks is of the same intensity or integral with the main peak, we discarded this set of experiments from future studies. We also tried a different amine but noted a slight shift in the principal peak and the appearance of a minor peak (Fig. 5B). The same observation was noted when an amino acid was incorporated (Fig. 5C). Last, we used **Zn-2-*RR*** and phenyl glycinol at high complex analyte ratios (1 : 100 and 1 : 150), but again, one single peak could be observed (Fig. 5D).

DFT studies

We performed a DFT study to investigate the species of **Zn-1-*RR*** formed in solution, to support the interpretation of the observed experimental signals (Scheme 4). Calculations were carried out to model the system in non-coordinating (chloroform) and coordinating (DMSO) solvent. To find the most relevant species, we screened the conformational space using CREST,[79] and re-optimised in Gaussian[80] the lowest and most representative minima at the B3LYP[81–83]-D3[84]/6-31g(d,p)[85,86] & SDD[87] level. The solvent (chloroform or DMSO) was modelled as a continuum media using PCM;[88,89] in some calculations, up to two DMSO explicit molecules were included (see Computational details in ESI†). Results in chloroform show that in the absence of an analyte or coordinating solvent, the optimised **Zn-1-*RR*** structure resembles that (**Dimer**) defined by single X-Ray diffraction. The **Dimer** is thermodynamically stable compared to two molecules of the corresponding **monomer** by 20.5 kcal mol^{-1}, suggesting the absence of the **Monomer** species in these conditions. However, two distinctive signals can be observed in the ^{19}F NMR experimentally (Fig. S7†). For this reason, we decided to reinvestigate the system, considering the possible presence of some water molecules, as this notion was noted during the preparation of the

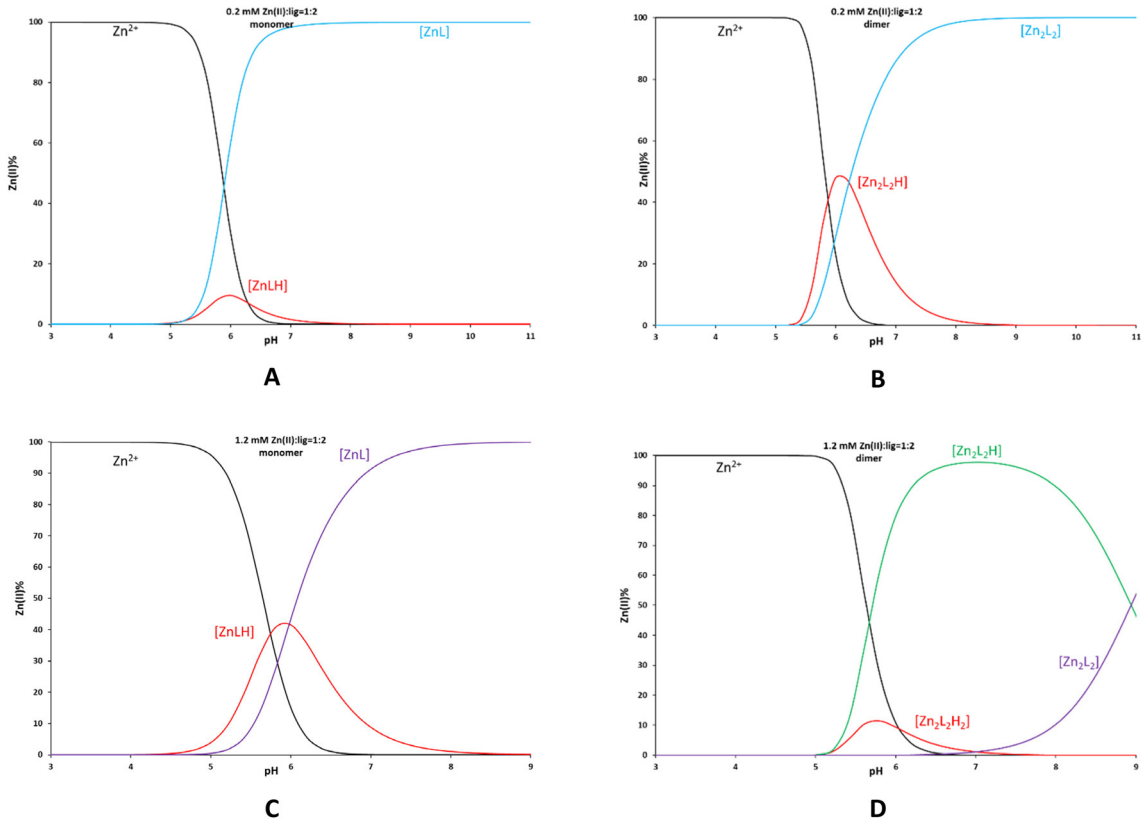

Fig. 4 Species distribution for the **Zn-2-*rac*** system at different concentrations (0.2 mM, A and B; 1.2 mM, C and D) with monomeric (A and C) and dimeric (B and D) models.

Table 2 pK values of **2-*rac*** in solutions of different concentrations (I = 0.2 M, T = 298 K, standard deviations are in parentheses). The pK_3 and pK_4 values at 1.2 mM is likely to be the same as for 0.2 mM

Ligand	**2-*rac***	
c[mM]	0.2	1.2
pK_1	4.27(9)	4.05(2)
pK_2	7.34(8)	7.40(3)
pK_3	9.50(6)	—
pK_4	10.99(4)	—

Ligand	**2-*rac***			
c[mM]	0.2		1.2	
ZnLH	19.20(12)	Fitting: 5.33×10^{-4}	19.47(12)	Fitting: 1.96×10^{-3}
ZnL	14.00(2)		13.49(11)	
$Zn_2L_2H_2$	—	Fitting: 6.98×10^{-4}	41.97(18)	Fitting: 5.02×10^{-4}
Zn_2L_2H	38.18(5)		36.9(3)	
Zn_2L_2	31.96(6)		27.96(11)	

complexes (see Fig. S2†). Different conformers of the **Monomer** and **Dimer** were optimised with one, two or three coordinating water molecules. This selection is because the Zn (II) coordination sphere can immediately change from 4 to 5 to 6 due to the presence of water molecules and/or Lewis bases. This flexibility has been explicitly described in biological and catalysis-related examples.[90,91] When one water molecule coordinates with the **Dimer**, it produces an intermediate species **Dimer(H_2O)**, which is 7.8 kcal mol^{-1} more stable; hence water coordination is favoured. For the **monomer**, the **Monomer (H_2O)** is favoured by 13.8 kcal mol^{-1}. However, the significant instability of the **monomer** compared to the **Dimer**, makes **Monomer(H_2O)** less stable than **Dimer(H_2O)** by 14.5 kcal mol^{-1}; hence this species could neither be experimentally

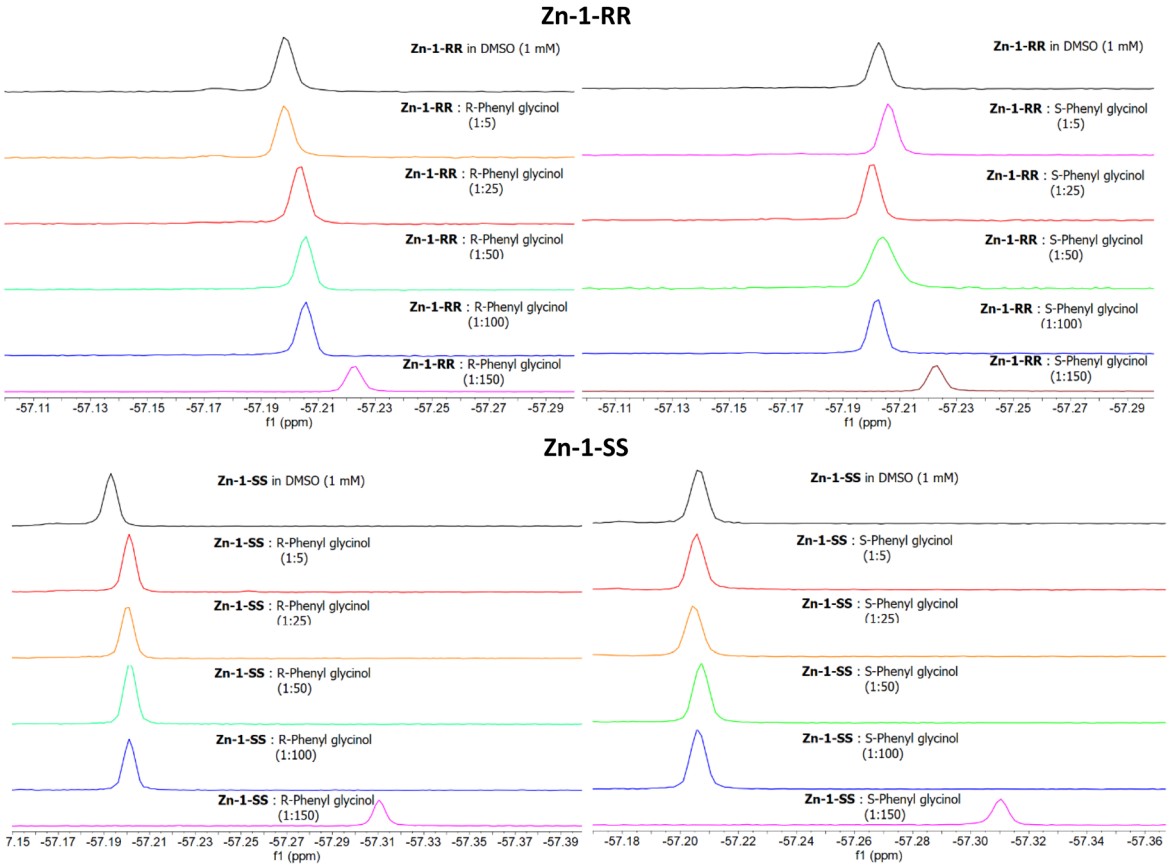

Fig. 5 ^{19}F NMR data for titration of **Zn-1*RR*** and **Zn-1-*SS*** with (*R* or *S*) phenylglycinol in different ratios *c* = 1 mM, *T* = 303 K.

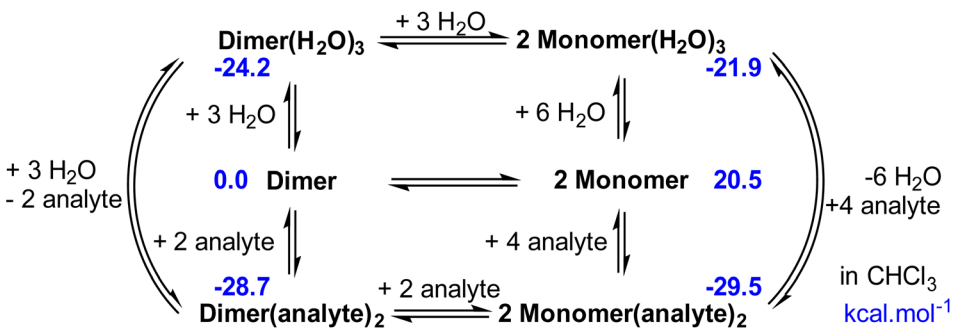

Scheme 4 Schematic representation of a simplified reaction network of the most relevant species and their relative free energies in chloroform and kcal mol^{-1}.

observed. Calculations accounting for two coordinating water molecules result in **Dimer(H$_2$O)$_2$** and **Monomer(H$_2$O)$_2$** with relative energies of −16.0 and −8.6 kcal mol^{-1}, respectively respect to **Dimer**. The coordination of this second water molecule reduces the difference between monomeric and dimeric species. However, the dimer is still preferred by 7.4 kcal mol^{-1}. The most stable isomer of **Monomer(H$_2$O)$_2$** presents a geometry with a water molecule coordinated to Zn and the other, forming a bridge between the oxygen of the ligand and the coordinated water. The geometry of this species suggests that a strong interaction with a third water molecule could be favoured. Calculations including a third water molecule yield **Dimer(H$_2$O)$_3$** and **Monomer(H$_2$O)$_3$** with relative energies of −24.2 and −21.9 kcal mol^{-1}, respectively respect to **Dimer**; see Scheme 4.

The difference between monomeric and dimeric species is small (2.3 kcal mol^{-1}), and depending on the water's concentration, both species could be observed. Please note that computational free energies reported corresponding to the 1 M Standard State. If we have concentrations significantly

different from 1 M, the energies alone cannot predict the formed species, and concentrations must be considered.[92] The overall equilibrium between these two species is governed by the chemical equation **Dimer(H_2O)$_3$** + 3 H_2O ⇌ 2 **Monomer(H_2O)$_3$**, this means that K_{eq} = [**Monomer(H_2O)$_3$**]^2/([**Dimer(H_2O)$_3$**][H_2O]^3) = 8.3. Hence at concentrations of water above [H_2O] = [**Monomer(H_2O)$_3$**]^2/([**Dimer(H_2O)$_3$**]K_{eq})$^{1/3}$, the monomer will be observed while below the dimer will be observed assuming there is enough water to form **Dimer(H_2O)$_3$**. We checked the monomer to total ratio as m/t = [**Monomer(H_2O)$_3$**]/[**Dimer**]$_0$ × 100 at different concentrations of water, where [**Dimer**]$_0$ is the initial concentration of dimer.

For initial concentrations of water [H_2O]$_0$ = 0.01, 0.1, 0.25 and 0.5 M, the predicted m/t ratio is 0.3%, 14%, 50% and 110%, suggesting that indeed in the reaction media, **Dimer(H_2O)$_3$** and **Monomer(H_2O)$_3$** could be present at the same time. Please note that as small errors in computational free energies will impact the equilibrium constants, we can only provide a qualitative explanation. The monomer–dimer equilibrium observed for initial water concentrations between 0.1 and 0.5 M could be at concentrations lower or higher.[93] The geometries of **Dimer(H_2O)$_3$** and **Monomer(H_2O)$_3$** are presented in Fig. 7. The most stable dimeric species presents a water molecule strongly coordinated to one of the Zn and another weakly coordinated to the other Zn, forming hydrogen bonds with the ligand (Zn–O distances 2.21 and 2.60 Å). The third water molecule bridges the strongly coordinated water molecule and one of the ligand's oxygens (OH–O distances are 1.61 and 1.74 Å). In the monomer, the structure presents one water molecule coordinated to the Zn and the other two bridges between the coordinated water and two oxygens of the ligand (OH–O(lig) distances are 1.69 and 1.65 Å and ZnO(H)H–O 1.71 and 1.72 Å). Adding more water molecules has not been considered as more strong interactions seem unlikely, and conformational complexity increases.

We also investigated the structures related to amines, considering the coordination of one and two analyte molecules, (*R*) 2-phenylglycinol, to the monomer and the dimer as hypothesised (Scheme 2). We found that **Dimer(analyte)**, **Monomer(analyte)** are located at −13.3 and −6.7 kcal mol^{-1} and **Dimer(analyte)$_2$**, and **Monomer(analyte)$_2$** at −28.7 and −29.5 kcal mol^{-1}, respectively; see Scheme 5 and Fig. 7. In this case, there is no space for the coordination of a third analyte molecule. Formation of **Monomer(analyte)$_2$** species is primarily favoured. The practical difficulties for sensing analytes at low concentrations seem to be due to the need for water–analyte

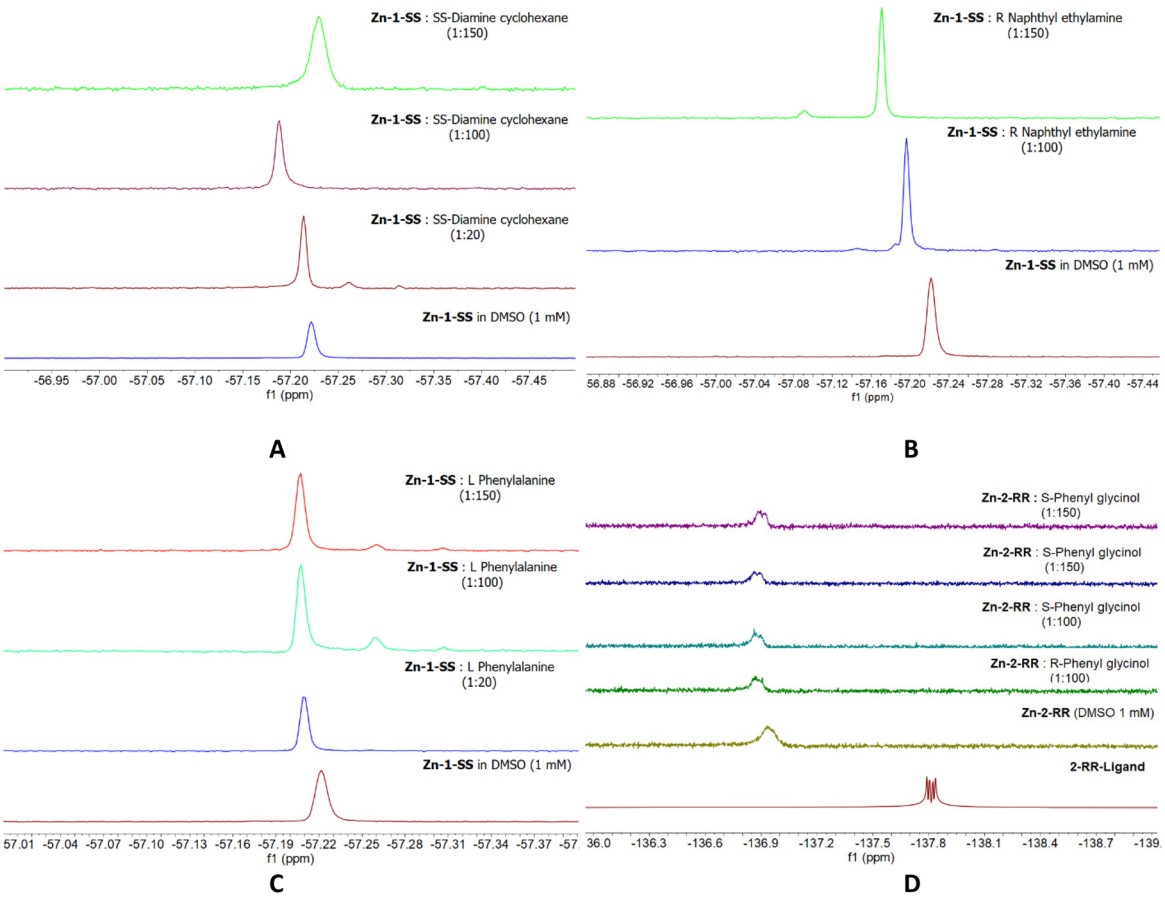

Fig. 6 ^{19}F NMR data of **Zn-1-*RR*** with various analytes *SS*-diaminocyclohexane A, *R* naphthyl ethylamine B, L – phenylalanine C, and **Zn-2-*RR*** with phenylglycinol (D) c = 1 mM, T = 303 K.

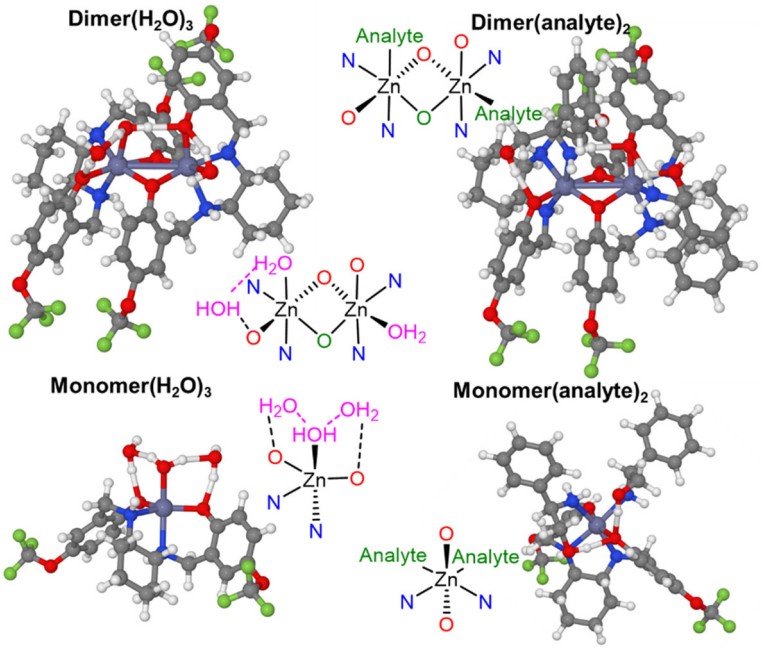

Fig. 7 Ball stick representation of the calculated structures of the **Dimer(H$_2$O)$_3$**, **Dimer(analyte)$_2$**, **Monomer(H$_2$O)$_3$** and **Monomer(analyte)$_2$**, in chloroform.

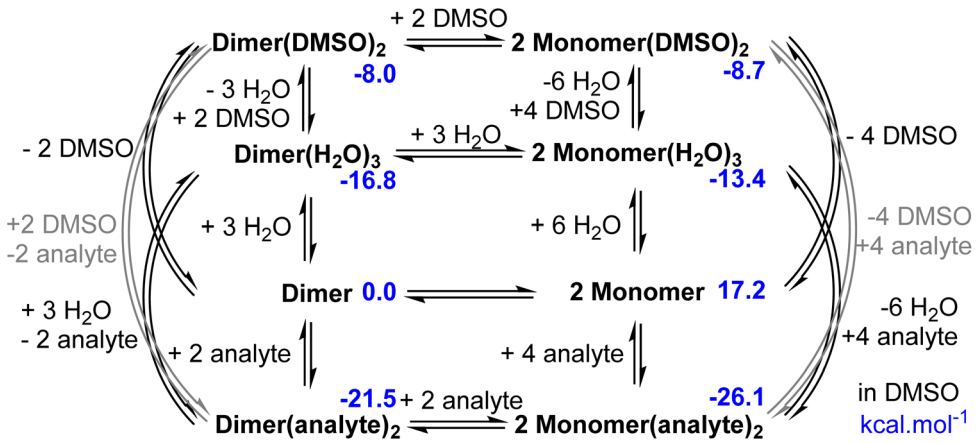

Scheme 5 Schematic representation of a simplified reaction network of the most relevant species and their relative free energies in DMSO and in kcal mol^{-1}.

exchange. The main chemical equations of the equilibria, in this case, are **Dimer(H$_2$O)$_3$** + 4 analyte ⇌ 2 **Monomer(analyte)$_2$** + 3 H$_2$O and **Monomer(H$_2$O)$_3$** + 2 analyte ⇌ 2 **Monomer (analyte)$_2$** + 3 H$_2$O. The energy difference between the aqua and analyte species is significant, 5.3 kcal mol^{-1} and 3.8 kcal mol^{-1}, respectively. In both cases, the expressions depend upon the concentration of water and analyte. The two equilibriums are related, as well as to the previously mentioned species. Hence, a system of 12 equations needs to be solved to find the concentration of all species at equilibrium (see ESI†). Using the concentration of water 0.5 M (an approximate value according to the results above), we tested the *a*/*t* ratio = [**Monomer(analyte)$_2$**]/([**Dimer**]$_0$) × 100 at the [analyte]$_0$ = [**Dimer**]$_0$, 10 × [**Dimer**]$_0$ and 100 × [**Dimer**]$_0$; the respective *a*/*t* ratios are 0.5%, 29% and 178% (please note the relation between dimer and monomer is **1** to **2**). These results show that the relationship between water/analyte concentrations impacts the sensing ability of the complexes.

Following experimental results, we explored the equilibria in DMSO. The above-presented minima were computationally reoptimised using DMSO as the solvent, and results are presented in Scheme 5. The different conformers for the dimeric and monomeric species with one and two DMSO molecules coordinated were also searched. We found that the coordination of a DMSO molecule to form **Dimer(DMSO)** is favoured by −5.7 kcal mol^{-1} and the inclusion of a second DMSO molecule

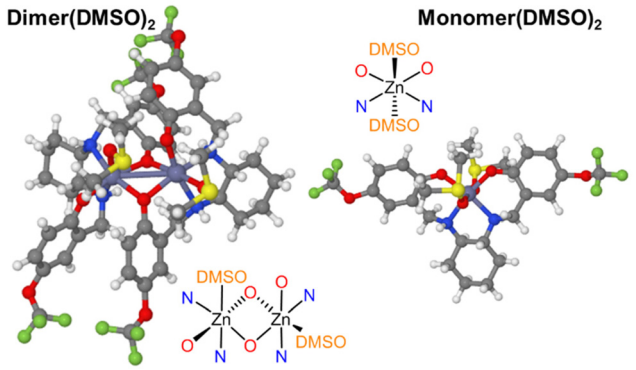

Fig. 8 Ball stick representation of the calculated structures of the **Dimer(DMSO)$_2$** and **Monomer(DMSO)$_2$**, in DMSO.

slightly stabilises the resulting **Dimer(DMSO)$_2$** to −8.0 kcal mol^{-1} in respect to the **Dimer**. The most stable conformer for **Dimer(DMSO)$_2$** is presented in Fig. 8, DMSO coordinates through the oxygen. The coordination of DMSO molecules also stabilises each **monomer**; the first DMSO stabilises the monomer in 7.6 kcal mol^{-1} and the second 5.4 kcal mol^{-1} more (see, Scheme 5 and Fig. 8). Hence, two **Monomer (DMSO)$_2$** molecules have similar energy as one **Dimer(DMSO)$_2$** (two monomers are 0.7 kcal mol^{-1} more stable). However, both are significantly less stable than the complexes with water or analyte molecules coordinated. Indeed, the most stable minimum is that of the **monomer (analyte)$_2$**, however the concentration of DMSO is several orders of magnitude larger than that of the analyte. The chemical equations, corresponding equilibrium constants, and mass balances were written to predict the concentration of all species at equilibria. Concentrations were obtained by solving a system of 19 equations and 19 unknown variables considering initial concentrations 14.06 M DMSO, 0.50 M water, 1 × 10^{-3} M Dimer, no concentration of the rest of species except for the analyte for which we considered 0, 1 × 10^{-3}, 1 × 10^{-2} and 0.1 M. At none or low concentration of analyte the most abundant species is **Mono(DMSO)$_2$**. Although this complex is less stable than the complexes with analyte and water, the large concentration of DMSO concerning the rest of the coordinating molecules (<0.5 M) makes the equilibria shift towards its formation. It is also interesting to note that although the stability of **Mono(DMSO)$_2$** and **Dimer(DMSO)$_2$** is similar, the chemical equation **Dimer(DMSO)$_2$** + 2 DMSO ⇌ 2 **Monomer(DMSO)$_2$** is also displaced towards the formation of **Monomer(DMSO)$_2$** for the same reason. At an increasing analyte concentration, the most abundant species becomes **monomer(analyte)$_2$**. The computational *a*/*t* ratio = [**Monomer(analyte)$_2$**]/([**Dimer**]$_0$) × 100 and *d*/*t* ratio = [**Monomer(DMSO)$_2$**]/([**Dimer**]$_0$)×100 at different initial concentrations of analyte [analyte]$_0$ = 0.0, 1 × 10^{-3}, 1 × 10^{-2} and 0.1 M are *a*/*t* = 0%, 2%, 87% and 198% and *d*/*t* = 192%, 190%, 108%, 2% explaining the difficulties associated to analyte sensing. Please note that in DMSO the concentration of water has an effect; decreasing the water concentration does not have a significant impact (*i.e.* [H$_2$O]$_0$ = 0.05 M results in *a*/*t* = 0%, 2%, 89% and 198% and *d*/*t* = 200%, 198%, 110%, 2% respectively for [analyte]$_0$ = 0.0, 1 10^{-3}, 1 10^{-2} and 0.1 M), but if the concentration of water is higher **Monomer (H$_2$O)$_3$** would be formed instead of **Monomer(DMSO)$_2$**. For instance, considering [H$_2$O]$_0$ = 5 M and [analyte]$_0$ = 1 × 10^{-2} M **Monomer(H$_2$O)$_3$** is formed and is more difficult to sense the analyte as the *a*/*t*, *d*/*t*, and *m*/*t* ratios are 7%, 6% and 186%. Increasing the concentration of analyte and considering [H$_2$O]$_0$ = 5 M and [analyte]$_0$ = 0.1 M **Monomer(analyte)$_2$** species is formed. These ratios change to *a*/*t*, *d*/*t*, and *m*/*t* 154%, 1% and 45%, respectively.

Discussion

The synthesis of the targeted families is straightforward, from commercially available resources and in two high-yielding steps. The compounds, as anticipated, are isolated as dimers;

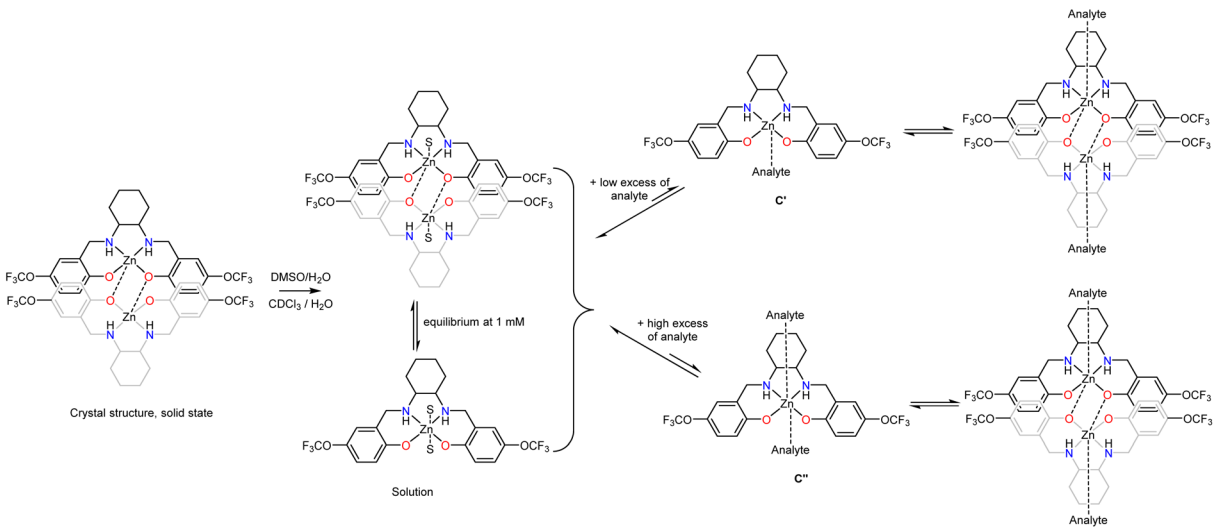

Scheme 6 A summarising schematic representation of our working hypothesis .

however, post-synthesis, they are susceptible to absorbing moisture (H_2O). In the solution phase, in the presence of coordinating solvents (DMSO or H_2O) and at a millimolar level (1 mM), NMR diffusion, solution and ESI† studies propose a dimer–monomer equilibrium; this finding is in contrast to known Zn-salen complexes which exist as monomers under similar conditions.[52,71] Variable temperature studies (NMR) would be insightful to elucidate at which temperature the monomeric or dimeric species will be favoured. Still, given that we aimed to develop an operational simple detection method, we did not proceed further.

We anticipated that coordinating solvent molecules, one or two, would occupy the vacant positions in the Zn coordination sphere and that slight excess of analyte would favour the formation of monomeric species **C′** or **C″**, respectively (Scheme 6), avoiding the presence other species (**A′** or **B′**, Scheme 2). By doing so, a new single distinct peak corresponding to **C′** or **C″** would appear in the NMR data, thus providing a new detection method (not two different peaks, one for the complex and one for the complex + analyte). However, the solvent-analyte exchange requires an extreme excess of the latter for a new distinct peak to appear in the ^{19}F NMR spectrum. The above evidence (Fig. 5 & 6) suggests that this approach may be suitable for diamines but cannot be generalised. For example, the excess of phenylglicinol results in complex decomposition, formation of the Zn(analyte)$_x$ complex and release of the fluorinated ligand (Fig. 5, **Zn-1-*SS*** 1 : 150 ratio).

Then, theoretical calculations were performed to shed light on the experimental findings. These calculations scrutinised the stability of all possible tetra-, penta- and hexa-coordinated Zn monomeric and dimeric species in the presence of coordinating and non-coordinating solvents and analytes. Different equilibriums are possible (Schemes 4 & 5), while speciation depends on concentration. The outcome favours unconventional hexa-coordinating species, which is a peculiar finding unsupported by the provided experimental evidence. However, these calculations explain that (a) the solvent-analyte exchange is energetically unfavourable and (b) the concentration of the H_2O molecules significantly impacts this process and prohibits the development of a new sensing process at low concentrations.

Conclusions

For the first time, we examined the ability of fluorine-based Zn-salan complexes to function as amine sensors with ^{19}F NMR. Being aware that these species will isolate as dimers, we aimed to obtain species **C′** or **C″** with slight analyte excess, but this process is unfavourable due to the presence of coordinating solvents. Future synthetic efforts will focus on altering the organic framework and having the antenna close to the metal centre to ease the sensing process in non-coordinating solvents.

Author contributions

GEK devised the project with critical input from NBE. NBE synthesised and characterised the ligands and complexes and performed the ^{19}F NMR sensing studies. GEK, GJT and SJC crystallographic data. AG and CK performed solution studies. YAH performed and helped with the evaluation of circular dichroism studies. RGM performed and evaluated MS studies. GRA performed diffusion ^{19}F NMR studies. MB performed theoretical calculations. All authors contributed to the preparation of the article.

Conflicts of interest

There are no conflicts to declare.

Acknowledgements

N. B. E. thanks the TETFUND for financial support. G. E. K. thanks the EPSRC UK National Crystallography Service at the University of Southampton for collecting the crystallographic data.[94] M. B. acknowledges financial support PID 2020-112762GB-I00 funded by MCIN/AEI/10.13039/501100011033. We thank Prof. Louise C. Serpell (Sussex Neuroscience) for accessing the Circular Dichroism (CD) apparatus.

References

1 E. Zor, H. Bingol and M. Ersoz, *Trends Anal. Chem.*, 2019, **121**, 115662.
2 D. S. Hassan, F. Y. Thanzeel and C. Wolf, *Chirality*, 2020, **32**, 457–463.
3 X. Liang, W. Liang, P. Jin, H. Wang, W. Wu and C. Yang, *Chemosensors*, 2021, **9**, 1–23.
4 F. Burg, S. Breitenlechner, C. Jandl and T. Bach, *Chem. Sci.*, 2020, **11**, 2121–2129.
5 C. Wolf and K. W. Bentley, *Chem. Soc. Rev.*, 2013, **42**, 5408–5424.
6 X. Niu, X. Yang, H. Li, J. Liu, Z. Liu and K. Wang, *Microchim. Acta*, 2020, **187**, 676.
7 C. M. Kisukuri and L. H. Andrade, *Org. Biomol. Chem.*, 2015, **13**, 10086–10107.
8 S. R. Laplante, L. D. Fader, K. R. Fandrick, D. R. Fandrick, O. Hucke, R. Kemper, S. P. F. Miller and P. J. Edwards, *J. Med. Chem.*, 2011, **54**, 7005–7022.
9 R. Jayakumar, R. Vadivel and N. Ananthi, *Org. Med. Chem. Int. J.*, 2018, **5**, 555661.
10 D. W. Armstrong, C. D. Chang and W. Y. Li, *J. Agric. Food Chem.*, 1990, **38**, 1674–1677.
11 Y. Hou, Z. Liu, L. Tong, L. Zhao, X. Kuang, R. Kuang and H. Ju, *Dalton Trans.*, 2019, **49**, 31–34.

12 X. Yu, L. He, M. Pentok, H. Yang, Y. Yang, Z. Li, N. He, Y. Deng, S. Li, T. Liu, X. Chen and H. Luo, *Nanoscale*, 2019, **11**, 15589–15595.
13 L. A. Warning, A. R. Miandashti, L. A. McCarthy, Q. Zhang, C. F. Landes and S. Link, *ACS Nano*, 2021, **15**, 15538–15566.
14 K. W. Bentley and C. Wolf, *J. Am. Chem. Soc.*, 2013, **135**, 12200–12203.
15 E. G. Shcherbakova, V. Brega, T. Minami, S. Sheykhi, T. D. James and P. Anzenbacher, *Chem. – Eur. J.*, 2016, **22**, 10074–10080.
16 Z. A. De los Santos, S. MacAvaney, K. Russell and C. Wolf, *Angew. Chem., Int. Ed.*, 2020, **59**, 2440–2448.
17 Z. A. De los Santos, C. C. Lynch and C. Wolf, *Angew. Chem., Int. Ed.*, 2019, **58**, 1198–1202.
18 K. W. Bentley, D. Proano and C. Wolf, *Nat. Commun.*, 2016, **7**, 12539.
19 J. M. Dragna, G. Pescitelli, L. Tran, V. M. Lynch, E. V. Anslyn and L. Di Bari, *J. Am. Chem. Soc.*, 2012, **134**, 4398–4407.
20 W. Yang, K. R. Cadwallader, Y. Liu, M. Huang and B. Sun, *Food Chem.*, 2019, **282**, 153–163.
21 Z. Liu, Y. Xu, C. Y. Ji, S. Chen, X. Li, X. Zhang, Y. Yao and J. Li, *Adv. Mater.*, 2020, **32**, 1–9.
22 S. R. Chaudhari and N. Suryaprakash, *Org. Biomol. Chem.*, 2012, **10**, 6410–6419.
23 Z. Xu, C. Liu, S. Zhao, S. Chen and Y. Zhao, *Chem. Rev.*, 2019, **119**, 195–230.
24 Z. Chen, M. Yang, Z. Sun, X. Zhang, J. Xu, G. Bian and L. Song, *Anal. Chem.*, 2019, **91**, 14591–14596.
25 C. Dong, Z. Xu, L. Wen, S. He, J. Wu, Q. H. Deng and Y. Zhao, *Anal. Chem.*, 2021, **93**, 2968–2973.
26 M. S. Seo and H. Kim, *J. Am. Chem. Soc.*, 2015, **137**, 14190–14195.
27 C. M. Puentes and T. J. Wenzel, *Beilstein J. Org. Chem.*, 2017, **13**, 43–53.
28 Z. Sun, Z. Chen, Y. Wang, X. Zhang, J. Xu, G. Bian and L. Song, *Org. Lett.*, 2020, **22**, 589–593.
29 C. C. Hinckley, *J. Am. Chem. Soc.*, 1969, **91**, 5160–5162.
30 J. A. Dale, D. L. Dull and H. S. Mosher, *J. Org. Chem.*, 1969, **34**, 2543–2549.
31 W. H. Pirkle, D. L. Sikkenga and M. S. Pavlin, *J. Org. Chem.*, 1977, **42**, 384–387.
32 J. Bravo, C. Cativiela, J. E. Chaves, R. Navarro and E. P. Urriolabeitia, *Inorg. Chem.*, 2003, **42**, 1006–1013.
33 J. X. Yu, R. R. Hallac, S. Chiguru and R. P. Mason, *Prog. Nucl. Magn. Reson. Spectrosc.*, 2013, **70**, 25–49.
34 J. Yu, V. Kodibagkar, W. Cui and R. Mason, *Curr. Med. Chem.*, 2005, **12**, 819–848.
35 M. A. Danielson and J. J. Falke, *Annu. Rev. Biophys. Biomol. Struct.*, 1996, **25**, 163–195.
36 E. N. G. Marsh and Y. Suzuki, *ACS Chem. Biol.*, 2014, **9**, 1242–1250.
37 M. G. Boersma, T. Y. Dinarieva, W. J. Middelhoven, W. J. H. Van Berkel, J. Doran, J. Vervoort and I. M. C. M. Rietjens, *Appl. Environ. Microbiol.*, 1998, **64**, 1256–1263.
38 Y. Zhao and T. M. Swager, *J. Am. Chem. Soc.*, 2015, **137**, 3221–3224.
39 Y. Zhao, L. Chen and T. M. Swager, *Angew. Chem., Int. Ed.*, 2016, **55**, 917–921.
40 W. Wang, X. Xia, G. Bian and L. Song, *Chem. Commun.*, 2019, **55**, 6098–6101.
41 Y. Shimazaki, in *Pure and Applied Chemistry*, Walter de Gruyter GmbH, 2014, vol. 86, pp. 163–172.
42 H. Nagae, R. Aoki, S. N. Akutagawa, J. Kleemann, R. Tagawa, T. Schindler, G. Choi, T. P. Spaniol, H. Tsurugi, J. Okuda and K. Mashima, *Angew. Chem., Int. Ed.*, 2018, **57**, 2492–2496.
43 I. Caretti, E. Carter, I. A. Fallis, D. M. Murphy and S. Van Doorslaer, *Phys. Chem. Chem. Phys.*, 2011, **13**, 20427–20434.
44 D. M. Murphy, I. Caretti, E. Carter, I. A. Fallis, M. C. Göbel, J. Landon, S. Van Doorslaer and D. J. Willock, *Inorg. Chem.*, 2011, **50**, 6944–6955.
45 B. Agrahari, S. Layek, R. Ganguly and D. D. Pathak, *New J. Chem.*, 2018, **42**, 13754–13762.
46 S. Mouri, Z. Chen, H. Mitsunuma, M. Furutachi, S. Matsunaga and M. Shibasaki, *J. Am. Chem. Soc.*, 2010, **132**, 1255–1257.
47 S. Shaw and J. D. White, *Chem. Rev.*, 2019, **119**, 9381–9426.
48 S. M. Kirk, P. McKeown, M. F. Mahon, G. Kociok-Köhn, T. J. Woodman and M. D. Jones, *Eur. J. Inorg. Chem.*, 2017, 5417–5426.
49 L. Chiang, K. Herasymchuk, F. Thomas and T. Storr, *Inorg. Chem.*, 2015, **54**, 5970–5980.
50 A. Thevenon, J. A. Garden, A. J. P. White and C. K. Williams, *Inorg. Chem.*, 2015, **54**, 11906–11915.
51 S. I. Sampani, V. Zdorichenko, M. Danopoulou, M. C. Leech, K. Lam, A. Abdul-Sada, B. Cox, G. J. Tizzard, S. J. Coles, A. Tsipis and G. E. Kostakis, *Dalton Trans.*, 2020, **49**, 289–299.
52 S. Di Bella, *Dalton Trans.*, 2021, **50**, 6050–6063.
53 R. Xu, L. Hua, X. Li, Y. Yao, X. Leng and Y. Chen, *Dalton Trans.*, 2019, **48**, 10565–10573.
54 T. Nakamura, S. Tsukuda and T. Nabeshima, *J. Am. Chem. Soc.*, 2019, **141**, 6462–6467.
55 G. Salassa, M. J. J. Coenen, S. J. Wezenberg, B. L. M. Hendriksen, S. Speller, J. A. A. W. Elemans and A. W. Kleij, *J. Am. Chem. Soc.*, 2012, **134**, 7186–7192.
56 I. P. Oliveri and S. Di Bella, *Chemistry*, 2023, **5**, 119–137.
57 N. Kelly, K. Schnaars, K. Gloe, T. Doert, J. J. Weigand and K. Gloe, *Aust. J. Chem.*, 2017, **70**, 601–607.
58 A. L. Singer and D. A. Atwood, *Inorg. Chim. Acta*, 1998, **277**, 157–162.
59 H. Adams, N. A. Bailey, D. E. Fenton, I. G. Ford, S. J. Kitchen, M. G. Williams, P. A. Tasker, A. J. Leong and L. F. Lindoy, *J. Chem. Soc., Dalton Trans.*, 1991, 1665–1674.
60 M. Karmakar, A. Frontera and S. Chattopadhyay, *CrystEngComm*, 2020, **22**, 6876–6885.

61 H. R. Wen, J. J. Hu, K. Yang, J. L. Zhang, S. J. Liu, J. S. Liao and C. M. Liu, *Inorg. Chem.*, 2020, **59**, 2811–2824.
62 S. Bunda, N. V. May, D. Bonczidai-Kelemen, A. Udvardy, H. Y. V. Ching, K. Nys, M. Samanipour, S. Van Doorslaer, F. Joó and N. Lihi, *Inorg. Chem.*, 2021, **60**, 11259–11272.
63 S. Bunda, K. Voronova, Á. Kathó, A. Udvardy and F. Joó, *Molecules*, 2020, **25**, 3993.
64 N. Lihi, S. Bunda, A. Udvardy and F. Joó, *J. Inorg. Biochem.*, 2020, **203**, 110945.
65 A. Böttcher, H. Elias, E. G. Jäger, H. Langfelderova, M. Mazur, L. Müller, H. Paulus, P. Pelikan, M. Rudolph and M. Valko, *Inorg. Chem.*, 1993, **32**, 4131–4138.
66 J. Devonport, J. Spencer and G. E. Kostakis, *Dalton Trans.*, 2021, **50**, 12069–12073.
67 F. H. Allen, *Acta Crystallogr., Sect. B: Struct. Sci.*, 2002, **58**, 380–388.
68 G. Li, X. Zhao, L. Wang and W. Liu, *ChemistrySelect*, 2019, **4**, 9317–9321.
69 J. Dong, C. Tan, K. Zhang, Y. Liu, P. J. Low, J. Jiang and Y. Cui, *J. Am. Chem. Soc.*, 2017, **139**, 1554–1564.
70 C. He, J. Wang, P. Wu, L. Jia, Y. Bai, Z. Zhang and C. Duan, *Chem. Commun.*, 2012, **48**, 11880–11882.
71 K. T. Hylland, S. Øien-Ødegaard, R. H. Heyn and M. Tilset, *Eur. J. Inorg. Chem.*, 2020, 3627–3643.
72 C. He, Z. Lin, Z. He, C. Duan, C. Xu, Z. Wang and C. Yan, *Angew. Chem., Int. Ed.*, 2008, **47**, 877–881.
73 Y. Jiao, J. Zhang, L. Zhang, Z. Lin, C. He and C. Duan, *Chem. Commun.*, 2012, **48**, 6022–6024.
74 Y. Liu, X. Wu, C. He, Z. Li and C. Duan, *Dalton Trans.*, 2010, **39**, 7727–7732.
75 Y. Li, L. Wen, H. Meng, J. Lv, G. Luo and Y. Zhao, *Cell Rep. Phys. Sci.*, 2020, **1**, 100100.
76 A. Böttcher, H. Elias, L. Müller and H. Paulus, *Angew. Chem., Int. Ed. Engl.*, 1992, **31**, 623–625.
77 A. W. Addison, T. N. Rao, J. Reedijk, J. Van Rijn and G. C. Verschoor, *J. Chem. Soc., Dalton Trans.*, 1984, 1349–1356.
78 R. Evans, Z. Deng, A. K. Rogerson, A. S. McLachlan, J. J. Richards, M. Nilsson and G. A. Morris, *Angew. Chem., Int. Ed.*, 2013, **52**, 3199–3202.
79 P. Pracht, F. Bohle and S. Grimme, *Phys. Chem. Chem. Phys.*, 2020, **22**, 7169–7192.
80 M. J. Frisch, G. W. Trucks, H. B. Schlegel, G. E. Scuseria, M. A. Robb, J. R. Cheeseman, G. Scalmani, V. Barone, G. A. Petersson, H. Nakatsuji, X. Li, M. Caricato, A. V. Marenich, J. Bloino, B. G. Janesko, R. Gomperts, B. Mennucci, H. P. Hratchian, J. V. Ortiz, A. F. Izmaylov, J. L. Sonnenberg, D. Williams, F. Ding, F. Lipparini, F. Egidi, J. Goings, B. Peng, A. Petrone, T. Henderson, D. Ranasinghe, V. G. Zakrzewski, J. Gao, N. Rega, G. Zheng, W. Liang, M. Hada, M. Ehara, K. Toyota, R. Fukuda, J. Hasegawa, M. Ishida, T. Nakajima, Y. Honda, O. Kitao, H. Nakai, T. Vreven, K. Throssell, J. A. Montgomery Jr., J. E. Peralta, F. Ogliaro, M. J. Bearpark, J. J. Heyd, E. N. Brothers, K. N. Kudin, V. N. Staroverov, T. A. Keith, R. Kobayashi, J. Normand, K. Raghavachari, A. P. Rendell, J. C. Burant, S. S. Iyengar, J. Tomasi, M. Cossi, J. M. Millam, M. Klene, C. Adamo, R. Cammi, J. W. Ochterski, R. L. Martin, K. Morokuma, O. Farkas, J. B. Foresman and D. J. Fox, *Gaussian 16, Revision C.01*, Gaussian, Inc., Wallin, 2016.
81 P. J. Stephens, F. J. Devlin, C. F. Chabalowski and M. J. Frisch, *J. Phys. Chem.*, 1994, **98**, 11623–11627.
82 C. Lee, W. Yang and R. G. Parr, *Phys. Rev. B: Condens. Matter Mater. Phys.*, 1988, **37**, 785–789.
83 A. D. Becke, *J. Chem. Phys.*, 1993, **98**, 5648–5652.
84 S. Grimme, *J. Comput. Chem.*, 2006, **27**, 1787–1799.
85 R. Ditchfield, W. J. Hehre and J. A. Pople, *J. Chem. Phys.*, 1971, **54**, 724–728.
86 P. C. Hariharan and J. A. Pople, *Theor. Chim. Acta*, 1973, **28**, 213–222.
87 M. Dolg, U. Wedig, H. Stoll and H. Preuss, *J. Chem. Phys.*, 1987, **86**, 866–872.
88 G. Scalmani and M. J. Frisch, *J. Chem. Phys.*, 2010, **132**, 114110.
89 J. Tomasi, B. Mennucci and R. Cammi, *Chem. Rev.*, 2005, **105**, 2999–3093.
90 N. J. Ataie, Q. Q. Hoang, M. P. D. Zahniser, Y. Tu, A. Milne, G. A. Petsko and D. Ringe, *Biochemistry*, 2008, **47**, 7673–7683.
91 J. L. Moore, J. Oppelt, L. Senft, A. Franke, A. Scheitler, M. W. Dukes, H. B. Alix, A. C. Saunders, S. Karbalaei, D. D. Schwartz, I. Ivanović-Burmazović and C. R. Goldsmith, *Inorg. Chem.*, 2022, **61**, 19983–19997.
92 M. Besora and F. Maseras, *Wiley Interdiscip. Rev.: Comput. Mol. Sci.*, 2018, **8**, e1372.
93 R. Pérez-Soto, M. Besora and F. Maseras, *Org. Lett.*, 2020, **22**, 2873–2877.
94 S. J. Coles and P. A. Gale, *Chem. Sci.*, 2012, **3**, 683–689.